AAS 23-220

OPTIMAL ORBITS FOR A RECYCLING STATION SUPPORTING IN-ORBIT RECYCLING

Maria Anna Laino* **and Massimiliano Vasile†**

This paper proposes a method to find the location of optimal orbits for a recycling station. The goal is to find the orbital elements of an orbit that can be reached from the regions of interest, for example where components of non-active spacecrafts are located. The idea is to look at areas in the orbital parameter space that are reached by propagating trajectories from the selected regions. Varying all initial parameters, sets of possible orbits are obtained. The associated manoeuvre cost is computed and compared to the classical direct transfers. The long-term evolution of the obtained orbits is studied to assess if they remain inside the reachable set. The orbits that minimise the manoeuvre cost are selected.

INTRODUCTION

The disposal of large structures in space at their end of life poses a very complex challenge. Structures of this type, such as Solar Power Satellites (SPSs), are modular and can operate almost indefinitely with the required repair and maintenance actions. To repair malfunctioning systems (or to create new ones), it is necessary to have the appropriate material available, that comes from the components of retired and no longer active spacecrafts, which will then be repurposed in an orbital station. In this context, it is necessary to identify the most populated regions in between Earth orbit and cis-lunar space where it is possible to find the material that it will then be transferred to the area of interest. These regions can be seen as the hubs of a transport network, all connected to a recycling station through low-cost transfers.

To date, no recycling station exists in space. This raises an unanswered question: what is the optimal orbit for a recycling station in space? A first solution could be that of a station in a Geosynchronous orbit (the proposed orbit for SPSs). This location, however, poses two main problems: it may not be easily accessible from the most distant hubs and above all, it would be dangerously close to protected regions. For this reason, this work analyses the possibility of finding an optimal location for a recycling station, which is easily accessible from all the hubs, exploiting the natural dynamics and impulsive manoeuvre.

The paper is organized into several sections. Initially, we introduce the dynamical model employed throughout this study, along with a mapping of the possible orbits based on their long-term evolution. Subsequently, we outline the transfer methods from a Geosynchronous orbit to the recycling station orbit while also presenting the reachable set of orbits from this region. The same type of analysis is performed for the transfer from a low-Earth orbit to the recycling station orbit, as well as for the transfer from a Moon Halo orbit. The suggested orbits and corresponding considerations are presented in the concluding sections.

*MSc, Department of Mechanical and Aerospace Engineering, University of Strathclyde, 75 Montrose Street, G1 1XJ, Glasgow, United Kingdom.

†Professor, Department of Mechanical and Aerospace Engineering, University of Strathclyde, 75 Montrose Street, G1 1XJ, Glasgow, United Kingdom

DYNAMICAL MODEL

In this work, a perturbed two-body dynamical model is utilised, in which the object is subject to the following equations of motion in vector form:

$$\ddot{\mathbf{r}} = -\frac{\mu}{r^3}\mathbf{r} + \mathbf{a}_{J_2} + \mathbf{a}_{\mathrm{s}} + \mathbf{a}_{\mathrm{m}} \tag{1}$$

where, μ is the gravitational parameter of the Earth*, $\mathbf{r} = [x,\ y,\ z]^\top$ denotes the position vector and r is its magnitude, x, y and z are the Cartesian coordinates in an Earth-Centered Inertial frame (ECI). The first term in Eq. (1) is the two-body acceleration term, while the other terms are, respectively, the accelerations coming from the J_2 zonal harmonic of the gravity field of the Earth and the Sun and Moon gravity.[1] Both the Sun and the Moon terms are obtained from their real ephemerides. The model was implemented in MATLAB R2022b and validated against the software GMAT.[2] The Matlab function `ode113` was used for the integration of the differential equations with a relative error tolerance set to 10^{-13} and absolute error tolerance set to 10^{-14}.

CARTOGRAPHY

For simplicity, the target orbit is assumed to be circular, characterised by the angles right-ascension of the ascending node or RAAN (Ω) and inclination (i) and by its radius (r). This choice is justified also by the need of frequent rendez-vous manoeuvres, which would be easier to handle in the case of a circular orbit. The selection of the final circular orbit starts with an examination of the long-term evolution of the orbital elements. This investigation aims to assess the stability of the orbit over time, whether the RAAN and inclination remain bounded and the orbit continues to be approximately circular (i.e., eccentricity close to zero), while also ensuring there are no impacts with the Moon, nor any possibilities of escape.

When only gravitational perturbations are considered, the average value of the semi-major axis of orbits remains constant in time. Allan & Cooke[3] demonstrated that for a model incorporating the second-order zonal harmonics of Earth's gravitational potential and the gravitational attraction of the Sun and Moon, assuming the lunar orbit lies in the ecliptic plane, an initially circular orbit will remain circular. Since the plane of the Moon's orbit is inclined at a mean angle of only 5.145 deg with respect to the ecliptic plane, one expects the eccentricity to exhibit small variations even within the framework of more realistic models that take accurate positions of the Moon and Sun. Thus, the orbital elements that could show moderate or large variations on long-time scales are the inclination and the RAAN. Indeed, it follows that the inclination and the RAAN can either librate around the point with $\Omega = 0\,\mathrm{deg}$, $i = i_{\mathrm{L}}(d)$, where $i_{\mathrm{L}}(d)$ is the inclination of the Laplace plane, or circulate, depending on the initial conditions, i.e. on the relative position between the pole of the orbital plane and the pole of the Laplace plane. The classical Laplace plane is the equilibrium solution for the averaged dynamics arising from Earth oblateness and luni-solar gravitational perturbation.[4] The plane of these uncontrolled circular orbits will precess about the pole of the Laplace plane in a predictable way. Figure 1 shows the inclination $i_{\mathrm{L}}(d)$ of the classical Laplace plane as a function of the distance d from the centre of the Earth. As it can be noted, $i_{\mathrm{L}}(d)$ tends to zero as d tends to zero and it tends to the inclination of the ecliptic plane (i.e., $23.44\,\mathrm{deg}$) as d increases.

To confirm the theoretical findings, a systematic scan was conducted running numerical propagations of the orbital elements of initially circular orbits for a duration of 100 years, starting from the

*The "Nomenclature" section at the end of the paper presents a comprehensive list and description of all the mathematical symbols used throughout the paper.

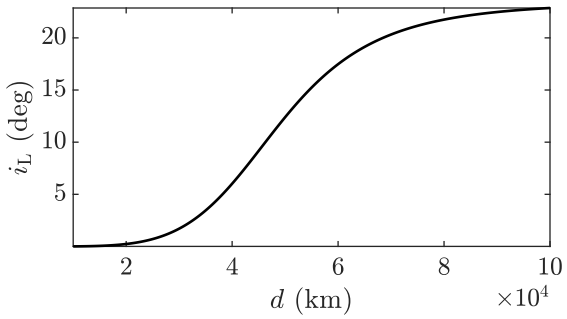

Figure 1: Inclination of the classical Laplace plane to Earth equator.

altitude of a Geosynchronous orbit (GSO) onwards. Figure 2 shows the librational and rotational motion in RAAN and inclination, which is the projection of the motion of the orbital pole, for some set of initial radii r_0 and inclinations i_0. While extensive numerical tests were performed across a wide range of initial conditions, for conciseness we present only a representative subset. Figure 3 shows the evolution of the eccentricity for the same set of initial conditions. As it can be noted, for initial conditions sufficiently close to the equilibrium solution the inclination and RAAN stay bounded and describe a closed curve around the Laplace plane. Nevertheless, beyond a certain altitude it can be observed that the variation in RAAN and inclination no longer follows a closed path around the Laplace plane and the eccentricity increases. Furthermore, at even higher altitudes, the influence of luni-solar perturbations is such that the orbit can approach the Moon closely, potentially resulting in impacts or fly-bys.

Some considerations can be made about the selection of the target circular orbit from a stability standpoint. A circular orbit can be chosen only in the case the altitude is low enough so that the orbital elements remain within specific bounds and the Moon's influence is not dominant. The numerical simulations show that the threshold value for the radius is $150\,000\,\mathrm{km}$. If a higher altitude is to be chosen, alternative options must be explored. A viable option is to consider orbits around the Lagrange points of the Earth–Moon or Sun–Earth system.[5] Notably, L_1, L_2, and L_3 are unstable points, whereas L_4 and L_5 offer stability (although for the Earth–Moon case, their stability is challenged by solar perturbations). Despite the instability of L_1 and L_2, numerous satellites currently occupy orbits in these regions, as they require minimal corrections for their trajectories. Table 1 shows the locations in space for the Lagrange points of the Sun–Earth and the Earth–Moon system.

	SE L_1	SE L_2	EM L_4	EM L_5
Distance (km)	1.498×10^6	1.508×10^6	3.84×10^5	3.84×10^5

Table 1: Distance of Lagrange points of Sun–Earth system (SE) and Earth–Moon (EM) from Earth.

GEOSYNCHRONOUS ORBIT TO RECYCLING STATION TRANSFER

In this study, we explore the hypothesis of placing the Solar Power Satellite in a GSO located in the Laplace plane.[6] Additionally, the Geostationary orbit (GEO) and the Graveyard orbit (approximately $300\,\mathrm{km}$ above GEO), are both densely populated regions in space where valuable material can be retrieved. Establishing a connection between the GSO region and the recycling station is

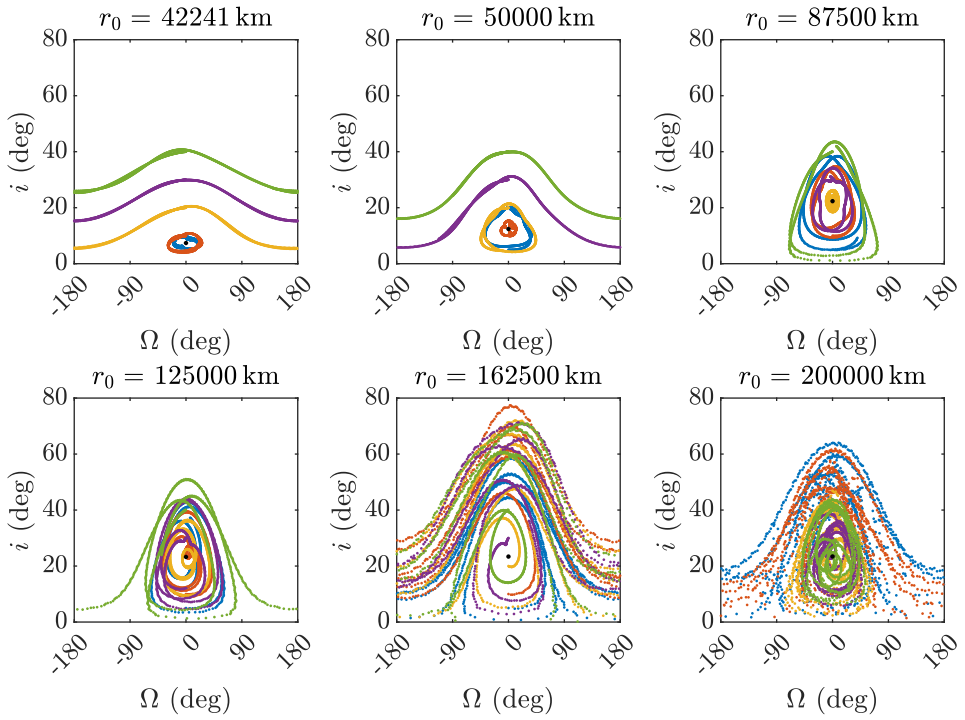

Figure 2: Long-term evolution of the orbital plane of circular orbits with initial radius r_0 and inclination i_0.

fundamental.

An essential criterion for selecting the optimal orbit, alongside stability and boundedness, is the manoeuvre cost required to reach the orbit from regions of interest. In this section, we assess the costs associated with various transfer methods from the GSO to circular orbits, including direct transfers and transfers that exploit luni-solar perturbations. The objective is to compare these approaches and identify the most cost-effective option for the intended mission.

Direct Transfer

The direct transfer is the classical two-impulses transfer. The first manoeuvre is executed to leave the initial orbit and enter an elliptical transfer orbit with perigee equal to the radius of the initial orbit and apogee equal to the radius of the final orbit. The second manoeuvre takes place at the apogee of the transfer orbit, it circularises the orbit and changes the inclination to match that of the final one. The manoeuvres should happen at the common line of nodes. Here, the hypothesis is that the two circular orbits share the same RAAN. It is worth noting that the perturbations are not considered in this analysis. In an actual mission scenario, such a transfer would not be realistic without accounting for perturbations, and it can be assumed that the required Δv would be larger to accommodate correction maneuvers.

Figure 4 represents the cost of the first manoeuvre (Δv_1), the cost of the second manoeuvre (Δv_2), the total transfer cost (Δv_{Tot}), and the total time of flight required for the transfer from the GSO,

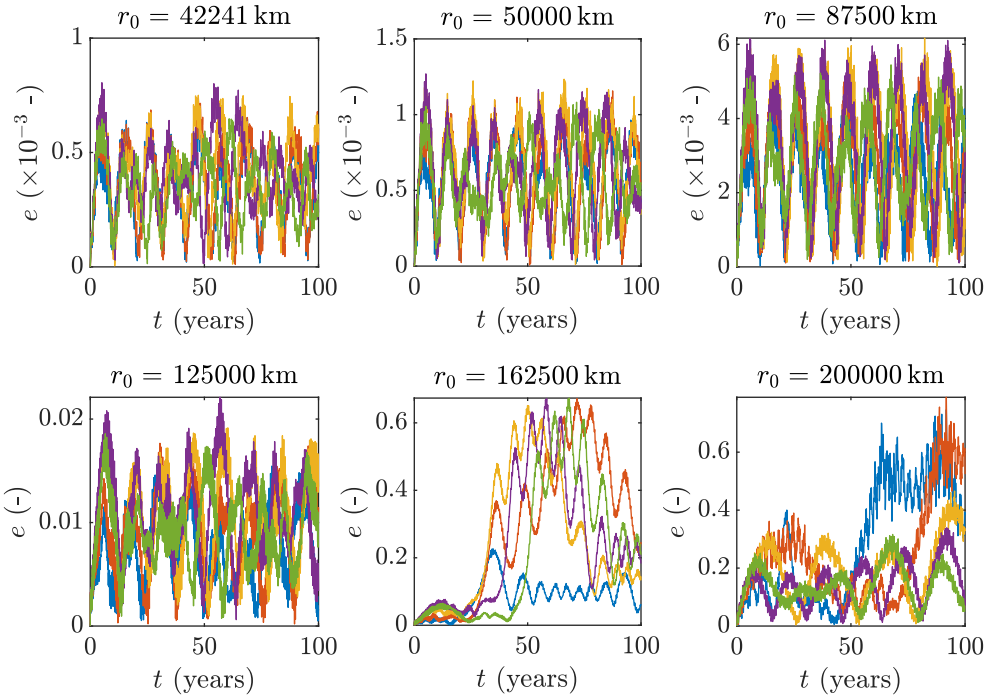

Figure 3: Long-term evolution of eccentricity of circular orbits with initial radius r_0 and inclination i_0 for time t.

with $\Omega_0 = 0\,\text{deg}$, $i_0 = 7.4\,\text{deg}$ and $r_0 = 42\,241\,\text{km}$, to a circular orbit characterized by inclination i and radius r.

Perturbation-assisted Transfer

This category of transfers differs from the direct approach due to the inclusion of perturbations. The aim is to leverage the variations in eccentricity and inclination caused by luni-solar perturbations to perform the transfers more efficiently. For example, the effect of these perturbations can aid in achieving the change of inclination required, completely or partially, thus reducing the overall fuel consumption required for a specific plane change manoeuvre.

A point on the GSO, with $\Omega_0 = 0\,\text{deg}$, $i_0 = 7.4\,\text{deg}$ and $r_0 = 42\,241\,\text{km}$, is chosen as the starting perigee point of a transfer orbit with radius of apogee r_a. The argument of perigee (ω_0) and the departing epoch (t_0) are varied in a range of values. The transfer orbit is propagated for a maximum time T_max. All apsis points along this transfer orbit are saved together with the corresponding orbital elements and time-of-flight. The osculating orbit resulting from the propagation of the set of initial conditions $[t_0,\, \omega_0,\, r_\text{a}]$ and corresponding to an apsis point is $\phi_\text{G}(t_0,\, \omega_0,\, r_\text{a})$, and will be characterized by a final Ω, i and r and time-of-flight. The manoeuvre costs to leave the GSO and enter the transfer orbit (Δv_1) and to enter the final circular orbit (Δv_2) are computed.

The procedure is run for a maximum propagation time $T_\text{max} = 1\,\text{year}$ starting from the following set of initial parameters:

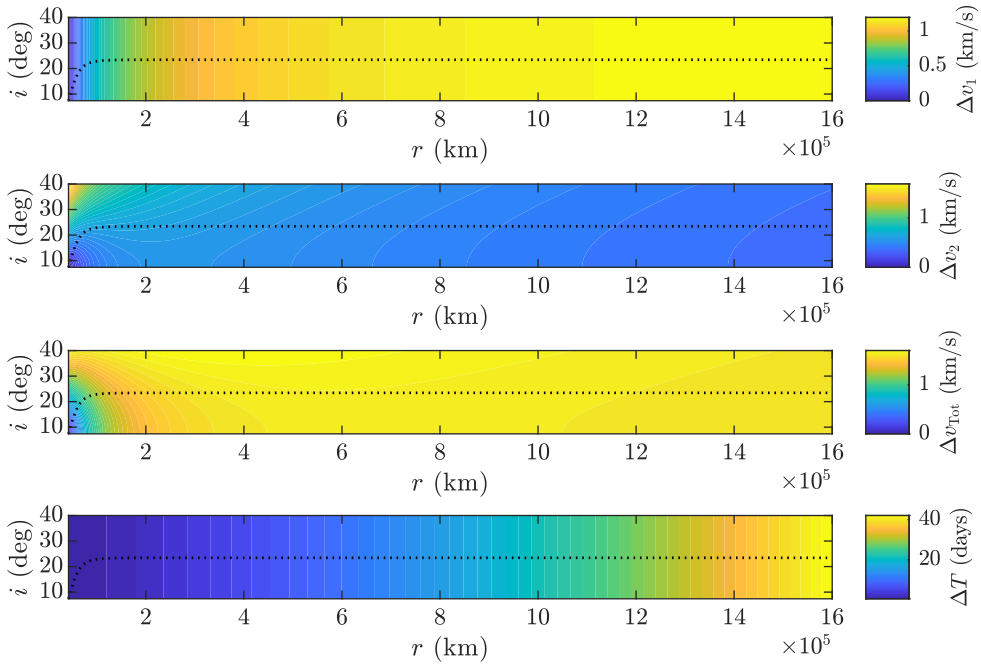

Figure 4: Cost of the first manoeuvre (Δv_1), second manoeuvre (Δv_2), total cost (Δv_{Tot}), and total time-of-flight necessary to transfer from a GSO to a circular orbit with inclination and radius i and r with a direct transfer. The dotted line represents the Laplace plane.

- $r_{\text{a}} =\in \{1, 1.5, 2, 2.5, 3, 5, 7, 10, 15\} \times 10^5\,\text{km}$.
- ω_0 varying from $0\,\text{deg}$ to $360\,\text{deg}$ with a $2\,\text{deg}$ step.
- t_0 fixed at 12:00:00 on the first day of each month in the year 2023.

REACHABLE SET FROM GEOSYNCHRONOUS ORBIT

In this section, the set of orbits reachable from the GSO of choice is presented. The solutions are divided in *bounded circular orbit solutions*, or the stable circular orbits with a radius below $150\,000\,\text{km}$, and the *Lagrange point solutions* or the orbits about the Lagrange points of the Sun–Earth and Earth–Moon system.

Bounded circular orbit solutions

The selection process is based on a two-step rationale. Firstly, we consider only the solutions that result in propellant savings compared to the direct approach. Once these potential solutions are identified, their long-term evolution is studied. This step helps us assess whether the selected solutions can be maintained over extended periods or if they are prone to instability.

Based on the Cartography study, circular orbits are considered bounded only when their radius is

below 150 000 km. Figure 5 illustrates the reachable circular orbits from a GSO using perturbation-aided transfers.

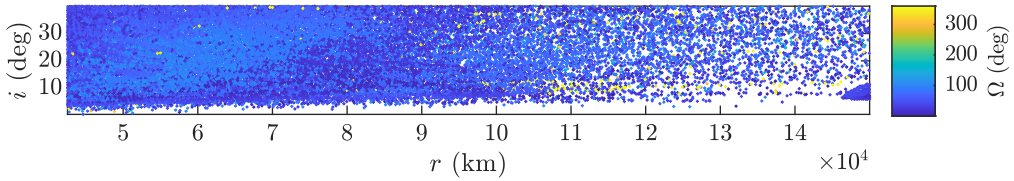

Figure 5: Osculating orbits ϕ_{G} below 150 000 km, resulting from perturbation-assisted transfers from the GSO.

The manoeuvre costs associated to the orbits ϕ_G in Figure 5 are compared with the corresponding direct transfer solutions, and in both instances, the mass of propellant consumed after each manoeuvre is computed as

$$\Delta m = m \left[1 - \exp\left(-\frac{\Delta v}{I_{\mathrm{s}} g_0} \right) \right] \tag{2}$$

where m is the mass of the spacecraft before the burn, I_{s} is the specific impulse, g_0 is the standard acceleration of gravity. In this analysis, an initial mass of 1000 kg is considered for the spacecraft and a specific impulse of 455 s.[1] The gains in total manoeuvre cost, total propellant mass consumed and time-of-flight are computed in absolute and relative terms as

$$\Delta x \text{ gain} = \Delta x_{\mathrm{d}} - \Delta x_{\mathrm{p}} \tag{3}$$

$$\Delta x \text{ gain} = \frac{\Delta x_{\mathrm{d}} - \Delta x_{\mathrm{p}}}{\Delta x_{\mathrm{d}}} \% \tag{4}$$

where x is a generic variable and the subscripts stand respectively for "direct" and "perturbed".

Only the solutions that show savings in terms of costs and propellant mass are retained. Figure 6 shows the gains in term of manoeuvre costs, propellant mass saved and time-of-flight. It is evident that only a limited number of solutions out of the wide range depicted in Figure 5 show savings compared to the direct transfer case. Moreover, the perturbation-aided transfers always require considerably longer transfer times.

Consider now the box $B = [i_{\mathrm{min}}, i_{\mathrm{max}}] \times [\Omega_{\mathrm{min}}, \Omega_{\mathrm{max}}] \times [r_{\mathrm{min}}, r_{\mathrm{max}}]$ with the boundary values $i_{\mathrm{min}}, i_{\mathrm{max}}, \Omega_{\mathrm{min}}, \Omega_{\mathrm{max}}, r_{\mathrm{min}}, r_{\mathrm{max}}$. We can define the reachable set as

$$\Psi = \{ B \mid i, \Omega, r \in B \}. \tag{5}$$

Specifically, the boundary values are fixed to $\Omega_{\mathrm{min}} = -45\,\mathrm{deg}$, $\Omega_{\mathrm{max}} = 45\,\mathrm{deg}$, $i_{\mathrm{min}} = 10\,\mathrm{deg}$, $i_{\mathrm{max}} = 40\,\mathrm{deg}$, while the condition on the radius is better expressed in terms of the maximum eccentricity, which shall remain below 0.01. These values align with the deviations observed in the long-term evolution analysis.

Once the reachable set is identified, the long-term evolution of each circular orbit is analysed in order to find the subset of orbits that remain inside the reachable set. This subset is defined as

$$\Psi_{\mathrm{C}} = \{ [\Omega, i, r] \mid [\Omega(T_{\mathrm{C}}), i(T_{\mathrm{C}}), r(T_{\mathrm{C}})] \in B \} \tag{6}$$

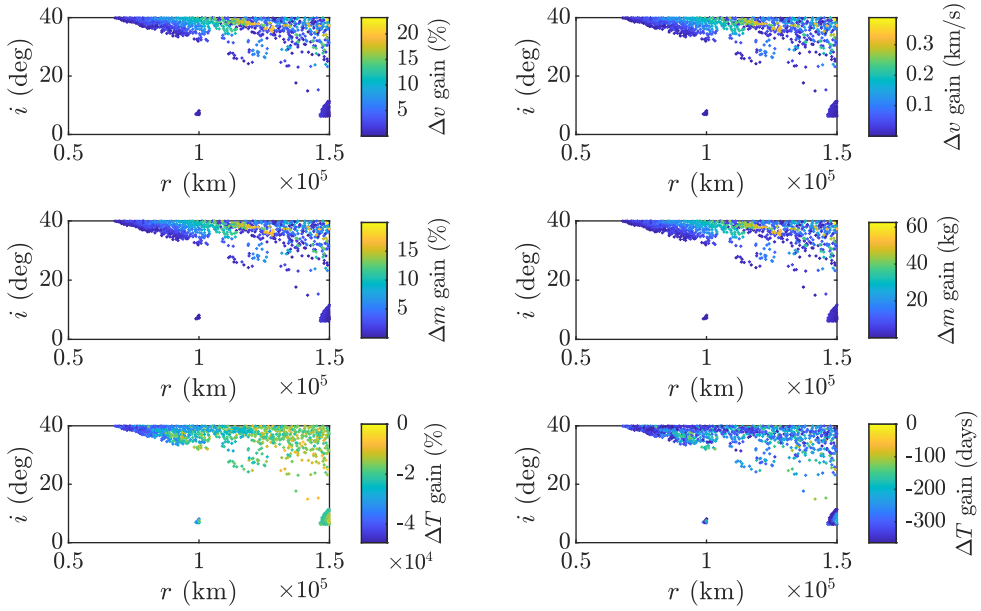

Figure 6: Osculating orbits ϕ_{G} below 150 000 km, with gains in term of manoeuvre costs (Δv), propellant mass consumed (Δm) and time-of-flight (ΔT).

where T_{C} is the time horizon over which we expect the orbit ϕ to remain in Ψ_{C}. For this analysis, $T_{\mathrm{C}} = 50$ years. A comprehensive long-term evolution analysis was performed on each circular orbit ϕ_{G} in Figure 6. The results are presented in Figure 7.

From the figure, it is evident that none of the orbits ϕ_{G} remain within the reachable set, leading to an empty set Ψ_{C}. This means that the condition on the type of transfer should be relaxed. Starting from a GSO, it is not advantageous to employ perturbation-aided transfers as the direct transfer already require a low total manoeuvre cost, as shown Figure 4. Future analysis should look into improving the estimation of the cost of direct transfers accounting for the effects of perturbations.

Lagrange point solutions

As mentioned in the previous section, two "families" of Lagrange points are considered in this work: Sun–Earth L_1 and L_2 and Earth–Moon L_4 and L_5. In this case, we simply want to verify if any of the solutions ϕ_{G} fall inside the vicinity of the points, hence we re-define the limits of reachable set Ψ. For the Sun–Earth L_1 and L_2, the boundary values of the reachable set are fixed to $\Omega_{\mathrm{min}} = -10\,\mathrm{deg}$, $\Omega_{\mathrm{max}} = 10\,\mathrm{deg}$, $i_{\mathrm{min}} = 23\,\mathrm{deg}$, $i_{\mathrm{max}} = 24\,\mathrm{deg}$, $r_{\mathrm{min}} = 1.398 \times 10^6\,\mathrm{km}$ and $r_{\mathrm{max}} = 1.608 \times 10^6\,\mathrm{km}$. Notably, none of the orbits ϕ_{G} are situated within the set Ψ. Again, different transfer solutions should be explored in this case.

On the other hand, for the Earth–Moon L_4 and L_5, the boundaries are set to $\Omega_{\mathrm{min}} = -15\,\mathrm{deg}$, $\Omega_{\mathrm{max}} = 15\,\mathrm{deg}$, $i_{\mathrm{min}} = 18.29\,\mathrm{deg}$, $i_{\mathrm{max}} = 28.59\,\mathrm{deg}$, $r_{\mathrm{min}} = 3.827 \times 10^5\,\mathrm{km}$ and $r_{\mathrm{max}} = 3.929 \times 10^5\,\mathrm{km}$. Figure 8 shows the orbits ϕ_{G} within the reachable set and the associated total cost (the sum of Δv_1 and Δv_2, previously defined). A small number of solutions are available, namely 11. This

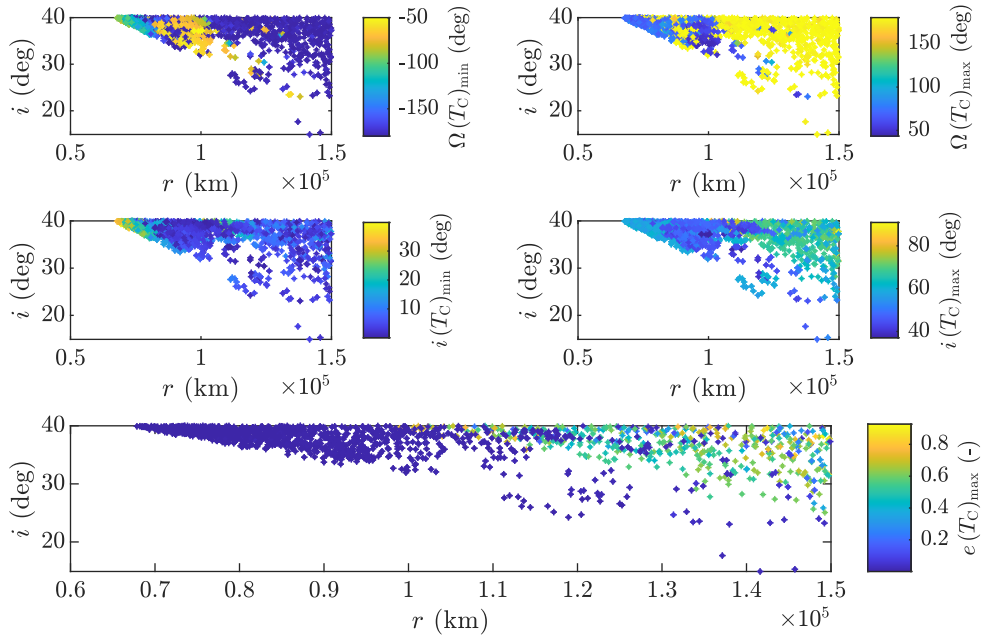

Figure 7: Osculating orbits ϕ_{G} below $150\,000\,\mathrm{km}$, with minimum and maximum RAAN and inclination and maximum eccentricity in the time horizon T_{C}.

implies that a connection from a GSO to one of these Lagrange point employing a perturbation-aided transfer is feasible. To get a better understanding, further analysis should look into the actual manoeuvre cost necessary to enter one of the orbits about the Lagrange points.

LOW EARTH ORBIT TO RECYCLING STATION TRANSFER

The Low Earth Orbit (LEO) is a densely populated region in space, making it a valuable resource for material retrieval. As such, it is essential to establish a connection between LEO and the recycling station orbit. Figure 9 shows the distribution of objects in LEO (Space-Track.org database, accessed $6/4/2023$) based on their semi-major axis (a) and inclination (i). As it can be noted, most objects are located in quasi-circular orbits. In contrast, the distribution of right-ascension of RAAN is pretty even. Our strategy for connecting LEO to the recycling station orbit will be based on a set of initial conditions consistent with this observed distribution. In a similar manner as in the previous section on the GSO, the costs of connecting a Low Earth Orbit (LEO) to a circular orbit using various transfer methods are evaluated.

Direct Transfer

Figure 10 and Figure 11 show the cost of the first manoeuvre (Δv_1), time-of-flight (ΔT) and second manoeuvre (Δv_2) of a direct transfer from a LEO with initial radius $r_0 = 7500\,\mathrm{km}$ and initial inclination i_0 ranging from 50 deg to 100 deg. For lower initial inclinations, increasing the radius of apogee to execute the change of plane manoeuvre would not result in a significant reduction in the final total Δv.[1]

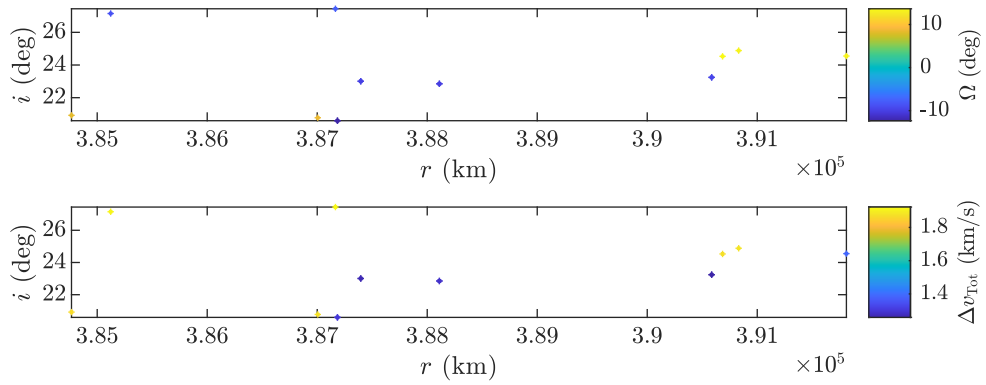

Figure 8: Osculating orbits ϕ_{G} falling inside the reachable set for the Earth–Moon L_4 and L_5 and associated total manoeuvre cost.

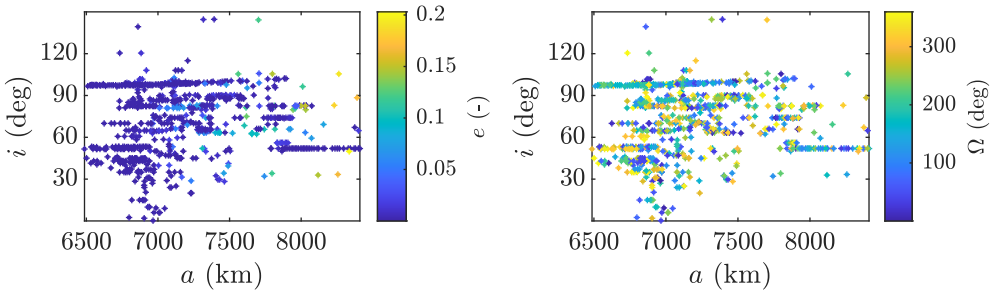

Figure 9: Distribution of objects in LEO.

Perturbation-assisted Transfer

Similarly to the GSO case, a point on a circular orbit in LEO is chosen as the starting perigee point of a transfer orbit with radius of apogee r_{a}. The RAAN (Ω_0), argument of perigee (ω_0) and the departing epoch (t_0) are varied in a range of values. The transfer orbit is propagated for a maximum time T_{max}. The apsis points along the transfer orbit are saved together with the corresponding orbital elements and time-of-flight. The osculating orbit resulting from the propagation of the set of initial conditions $[t_0,\, \Omega_0,\, \omega_0,\, r_{\mathrm{a}}]$ is $\phi_{\mathrm{L}}(t_i,\, \Omega_0,\, \omega_0,\, r_{\mathrm{a}})$, and will be characterized by a final Ω, i and r. The manoeuvre cost to leave the LEO and enter the transfer orbit ($\Delta v_{\mathrm{L}\,1}$) and to enter the final circular orbit ($\Delta v_{\mathrm{L}\,2}$) are computed and the time-of-flight (ΔT_{L}) is saved.

This procedure was implemented for a circular orbit with radius $r_0 = 7500\,\mathrm{km}$, maximum propagation time $T_{\mathrm{max}} = 1\,\mathrm{year}$ and the following initial parameters:

- $r_{\mathrm{a}} \in \{3, 5, 7, 10, 15\} \times 10^5\,\mathrm{km}$.
- Ω_0 and ω_0 varying from $0\,\mathrm{deg}$ to $360\,\mathrm{deg}$ with a step of $2\,\mathrm{deg}$.
- t_0 fixed at 12:00:00 on the first day of each month in the year 2023.

The outcome of this procedure will be presented in the upcoming sections.

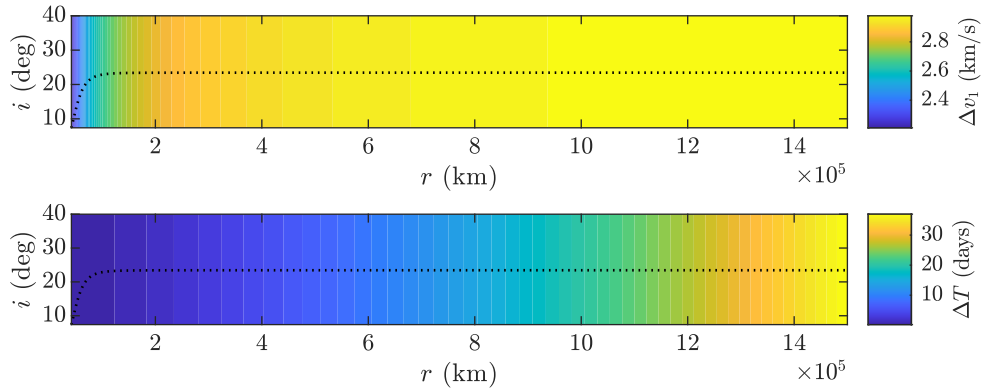

Figure 10: Cost of the first manoeuvre (Δv_1) and time-of-flight (ΔT) necessary to transfer from a circular LEO with radius r_0 to a circular orbit with inclination and radius i and r with a direct transfer. The dotted line represents the Laplace plane.

MOON HALO ORBIT TO RECYCLING STATION TRANSFER

In recent years, there has been a significant growth in interest in lunar exploration and study. Also, the idea of manned exploration has become popular with the concept of the Lunar gateway among the others, a small space station intended to orbit a Near-Rectilinear Halo Orbit (NRHO) about Lagrange point L_2 of the Earth–Moon system.[7] The Lagrange points are advantageous locations for space missions, in particular Earth–Moon L_2 could serve as a gateway to other destinations in the Solar System, or it could be used as a communication link between the Earth and the hidden side of the Moon.[8] Given the anticipated increase in activity and congestion at this location in the future, it holds good potential as a resource for material for the recycling station. A smart approach for transferring from the Lagrange points involves the utilisation of invariant manifold structures, as demonstrated in the Genesis mission profile within the Earth–Sun system.[8] These manifolds offer a cost-effective means of travelling in space.

Manifold Transfer

The invariant manifolds are peculiar to the periodic orbits in the circular restricted three-body problem (CR3BP), like Halo orbits about the Lagrange points L_1 and L_2.[5] Stable/unstable manifolds are phase space structures comprising vectors whose future/past positions converge to the orbit. If a spacecraft is on a stable manifold, its trajectory will converge towards the orbit, whereas if it is on the unstable one, it will diverge away from it. For a more detail analysis on the CR3BP, periodic orbits and invariant manifolds, it is advised to consult the original work by Koon et al.[5]

A point on a Halo orbit is chosen as the starting point of the invariant manifold. The trajectory is propagated in the perturbed dynamical model previously presented, for a maximum time T_{max}, directed both towards the interior and exterior of the three-body system. All apsis points along the manifold are recorded. The osculating orbit will be $\phi_{\text{M}}(t_0,\, \theta_0,\, A_z)$, resulting from the propagation of the initial conditions $[t_0,\, \theta_0,\, A_z]$, where θ_0 is the starting point along the Halo orbit (it can be seen as a "true anomaly", but starting from the right-most point of the orbit and proceeding in clockwise direction) and A_z is out-of-plane amplitude that defines the specific starting Halo orbit. While the manoeuvre cost to leave the Halo orbit is practically null, the cost to enter the final circular orbit

(Δv_{M}) is computed and the time-of-flight (ΔT_{M}) is saved.

The procedure was implemented for Earth–Moon L_2 southern (the maximum amplitude is in the $-z$ direction) Halo orbits, with:

- 100 Halo orbits, characterised by amplitude A_z varying from zero to ca. $75\,000\,\mathrm{km}$.
- θ_0 varying from 0 deg to 360 deg, with a step of 2 deg.
- t_0 fixed at 12:00:00 for the dates 9/3/2025, 16/3/2025, 23/3/2025, 30/3/2025, 28/5/2030, 4/6/2030, 11/6/2030, 18/6/2030, 26/12/2034, 2/1/2035, 9/1/2035, 16/1/2035. These dates were chosen to encompass the full range of variations in the position and inclination of the Moon. Specifically, the dates correspond to lunar inclination spanning across $28.59\,\mathrm{deg}$, $23.44\,\mathrm{deg}$, and $18.29\,\mathrm{deg}$.

The outcome of this procedure will be presented in the next sections.

REACHABLE SET FROM LEO AND MOON HALO ORBITS

Here, the set of orbits reachable from LEO and from the Moon Halo orbits is presented, following the same structure and rationale as in the previous GSO case.

Figure 12 shows all the orbits that can be reached from the LEO with a Perturbation-aided transfer and from the Moon Halo orbits with a manifold transfer.

Bounded circular orbit solutions

After all trajectories are propagated, two datasets are found that contain all osculating orbits ϕ_{L} and ϕ_{M}. A nearest neighbour search[†] is used to find all the matching orbits in these sets, or neighbouring points, which means that all the orbits from the sets that have RAAN, inclination and radius within a certain tolerance are kept, while the others are discarded. Here, the tolerance in the $[\Omega,\, i]$ plane is $1\,\mathrm{deg}$, while the tolerance in radius is $10\,\mathrm{km}$.

Figure 13 shows all the solutions with radius below $150\,000\,\mathrm{km}$.

The gains, defined as in Eq.(3) and Eq.(4) comparing LEO perturbation-aided transfers and direct transfers are computed and depicted in Figure 14. Here, only the solutions that show positive savings in terms of costs and propellant mass are retained. In contrast to the GSO case, a larger number of solutions is available. The savings in propellant mass are up to 100 kg. This is because the perturbation-aided transfers eliminate the cost of the change of inclination manoeuvre, which in this case is performed exclusively by the Sun and the Moon. However, this advantage comes at the expense of longer transfer times, which can extend up to a year compared to a maximum of about 40 days in the case of a direct transfer.

At last, solutions are propagated for $T_{\mathrm{C}} = 50\,\mathrm{years}$ to assess if they remain inside the reachable set, as defined in Eq.(5) and Eq.(6). The results are shown in Figure 15. In this case, nearly 2500 solutions are accessible.

Hence, some considerations can be drawn about the circular orbit solutions that minimise the manoeuvre cost. Figure,16 presents the costs and time-of-flight for solutions within the set Ψ_{C},

[†] https://uk.mathworks.com/help/stats/nearest-neighbors-1.html

originating from Low Earth Orbit (LEO) using a perturbation-aided transfer, Moon Halo orbits employing a manifold transfer, and Geostationary Orbit (GSO) via a direct transfer (as previously noted, employing a perturbation-aided transfer for the GSO case does not yield any advantage over a direct one). The solutions that allow to minimise the overall total Δv across the three regions are the ones located in the south-east region of the $[r,\, i]$ plane, around $r = 100\,000\,\mathrm{km}$ and $i = 20\,\mathrm{deg}$, while the RAAN spans between $-40\,\mathrm{deg}$ and $40\,\mathrm{deg}$. It is worth noting that within this interval, solutions arise from the whole range of initial inclinations in LEO (from 50 deg to 100 deg) and from Halo orbits ranging from the minimum to the maximum amplitude.

A last observation shall be made about the time-of-flight. Surely, the savings in propellant mass and manoeuvre cost are offset by significantly longer transfer durations. This trade-off is acceptable given that low-thrust solutions require transfer times in the same order of magnitude if not higher. Nevertheless, we isolated the solutions that require less than 150 days for both the LEO and Moon Halo orbit cases, as illustrated in Figure 17.

Lagrange point solutions

Figure 18 shows the orbits inside ϕ_{L} and ϕ_{M} inside the Sun–Earth reachable set and associated total cost, Figure 19 shows the same solutions for the Earth–Moon reachable set. A large number of solutions is available in both cases. This implies that Lagrange point regions can be easily connected with LEO and Moon Halo orbits via perturbation-aided transfers and manifold transfers. For a future extension to this work, it is essential to investigate the manoeuvre cost required for insertion into any of the orbits about the Lagrange points.

CONCLUSION

This paper presents a novel approach for identifying optimal orbits to locate recycling stations. Initially, a comprehensive assessment of the long-term orbital evolution was conducted to investigate the stability of possible orbits. It was found that a circular Earth orbit should have a radius below $150\,000\,\mathrm{km}$ to be bounded or other options, like orbits about the Lagrange points in the Sun–Earth and Earth–Moon system should be investigated.

We searched for a set of orbits reachable, at low Δv cost, from the GSO, LEO and Moon regions by exploiting a combination of natural dynamics and impulsive manoeuvres. Different transfer methods were proposed: for the GSO and LEO, direct bi-impulsive transfers and perturbation-aided transfer, or transfers that leverage the variations in orbital elements mainly caused by luni-solar perturbations. For the Moon Halo orbit case, invariant manifolds were employed. The reachable set of solutions was divided in "bounded circular orbit solutions", namely the solutions with radius below $150\,000\,\mathrm{km}$ and Lagrange point solutions, and in both instances a reachable set was defined, bounding the solutions in terms of RAAN, inclination and radius.

For the GSO to bounded circular orbits case, it was found that only in few instances the perturbation-aided transfers outperform the direct bi-impulsive approach, and of the remaining set of orbits none of them stays inside the reachable set for a time horizon of 50 years. For the Lagrange point solutions, instead, we simply aimed at assessing if any of the osculating orbits obtained would fall in the region of Sun–Earth L_1 and L_2 and Earth–Moon L_4 and L_5, leaving a more detailed analysis for future extensions. In the two cases, respectively none and very few orbits give approach the desired region.

In the context of transfers from LEO and Moon Halo orbits, a similar methodology was applied. Bounded circular solutions that outperform the direct transfer and remain inside the reachable set for 50 years were found. Notably, solutions minimizing the overall Δv are concentrated around a radius of $100\,000\,\mathrm{km}$, inclination of $20\,\mathrm{deg}$, and RAAN ranging from $-40\,\mathrm{deg}$ to $40\,\mathrm{deg}$. Despite longer transfer times required compared to a direct approach, some solutions within this set exhibit a time-of-flight under 150 days. For the Lagrange point solutions, a large number of the osculating orbits departing from LEO and from Moon Halo orbits effectively reach the desired region. Future analysis should investigate more in detail this option, assessing the cost necessary for insertion into Lagrange point-orbits.

ACKNOWLEDGMENT

This research was developed with the support of the ESA OSIP PROJECT "CORES: COllaborative REcycling of end-of-life Solar power satellites", Discovery EISI Agreement 4000136018, project officer Moritz Fontaine. The authors want to thank Catalin Gales and Roberto Paoli for their help on a previous version of this work.

NOMENCLATURE

ΔT	Time-of-flight
Δv	Manoeuvre cost
Ω	Right ascension of the ascending node
ω	Argument of perigee
ϕ	Osculating orbit
Ψ	Reachable set
θ_0	Starting point along Halo orbit
a	Semi-major axis
A_z	Out-of-plane amplitude
e	Eccentricity
i	Inclination
I_s	Specific impulse
L_i	Lagrange point
r	Radius
r_a	Radius of apogee

REFERENCES

[1] H. Curtis, *Orbital mechanics for engineering students*. Butterworth-Heinemann, 2013.

[2] S. P. Hughes, "General mission analysis tool (GMAT)," tech. rep., NASA Goddard Space Flight Center Greenbelt, 2016.

[3] R. Allan and G. Cook, "The long-period motion of the plane of a distant circular orbit," *Proceedings of the Royal Society of London. Series A. Mathematical and Physical Sciences*, Vol. 280, No. 1380, 1964, pp. 97–109.

[4] A. J. Rosengren, D. J. Scheeres, and J. W. McMahon, "The classical Laplace plane as a stable disposal orbit for geostationary satellites," *Advances in Space Research*, Vol. 53, No. 8, 2014, pp. 1219–1228.

[5] W. S. Koon, M. W. Lo, J. E. Marsden, and S. D. Ross, "Dynamical systems, the Three-Body Problem and space mission design," *Equadiff 99: (In 2 Volumes)*, pp. 1167–1181, World Scientific, 2000.

[6] I. McNally, D. Scheeres, and G. Radice, "Locating large solar power satellites in the geosynchronous Laplace plane," *Journal of Guidance, Control, and Dynamics*, Vol. 38, No. 3, 2015, pp. 489–505.

[7] D. C. Davis, F. S. Khoury, K. C. Howell, and D. J. Sweeney, "Phase control and eclipse avoidance in near rectilinear halo orbits," *AAS Guidance, Navigation and Control Conference*, No. JSC-E-DAA-TN77422, 2020.

[8] E. Canalias, G. Gomez, M. Marcote, and J. J. Masdemont, "Assessment of mission design including utilisation of libration points and weak stability boundaries," Tech. Rep. 03-4103a, European Space Agency, the Advanced Concepts Team, 2004. Available on line at www.esa.int/act.

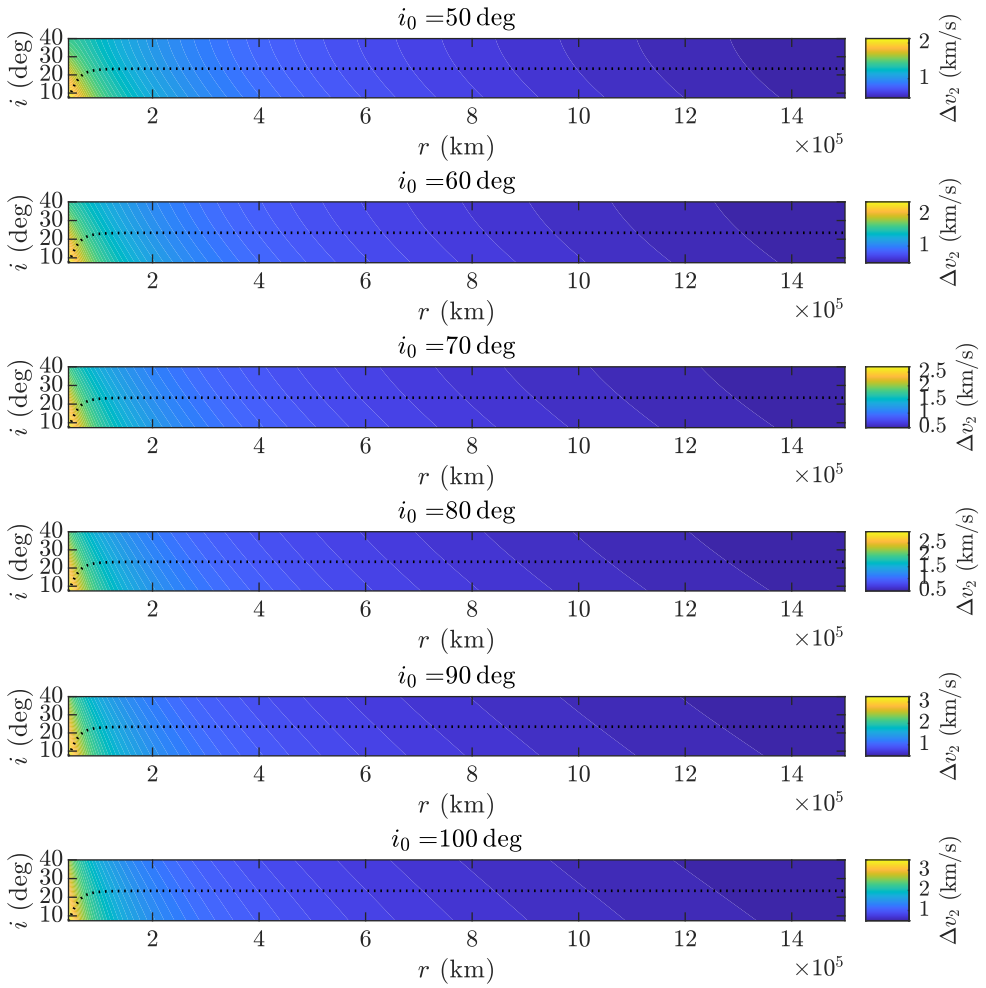

Figure 11: Cost of the second manoeuvre (Δv_2) necessary to transfer from a LEO with initial inclination i_0 and radius r_0 to a circular orbit with inclination and radius i and r with a direct transfer. The dotted line represents the Laplace plane.

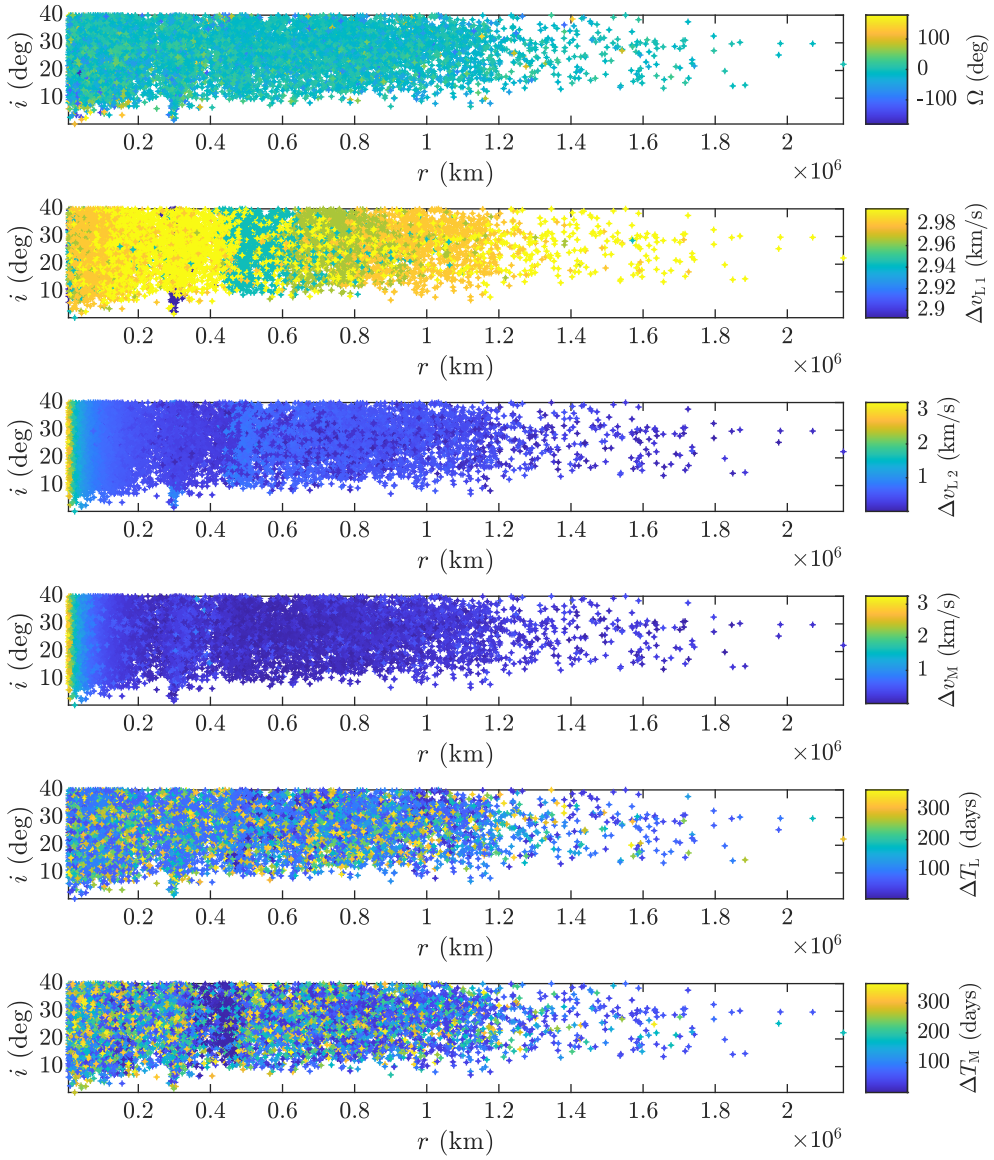

Figure 12: Osculating orbits ϕ_{L} and ϕ_{M}, resulting from perturbation-assisted transfers from LEO and manifold transfers from Moon Halo orbits, with manoeuvre costs and time-of-flight.

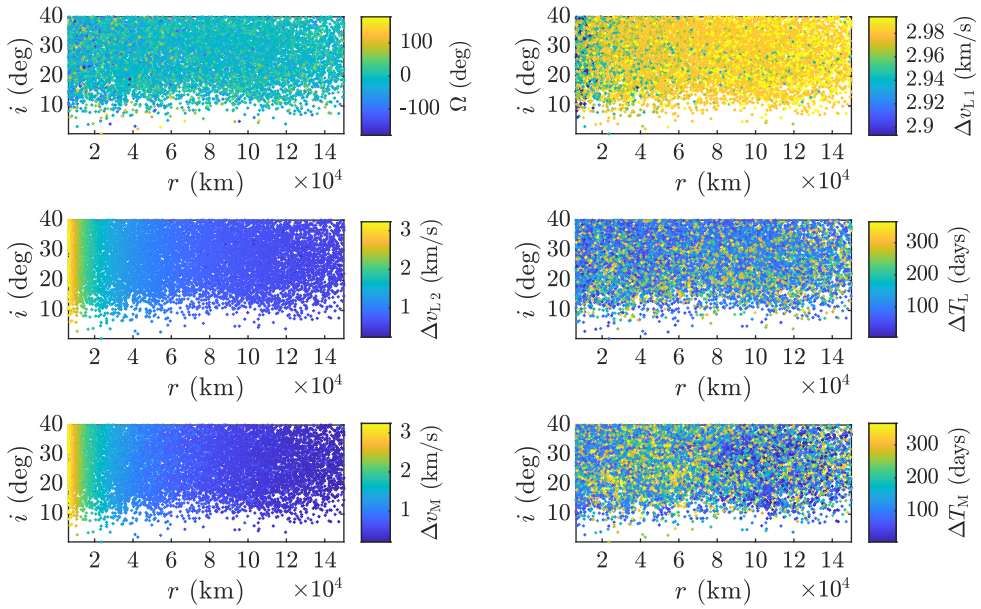

Figure 13: Osculating orbits ϕ_{L} and ϕ_{M} below 150 000 km, resulting from perturbation-assisted transfers from LEO and manifold transfers from Moon Halo orbits, with manoeuvre costs and time-of-flight.

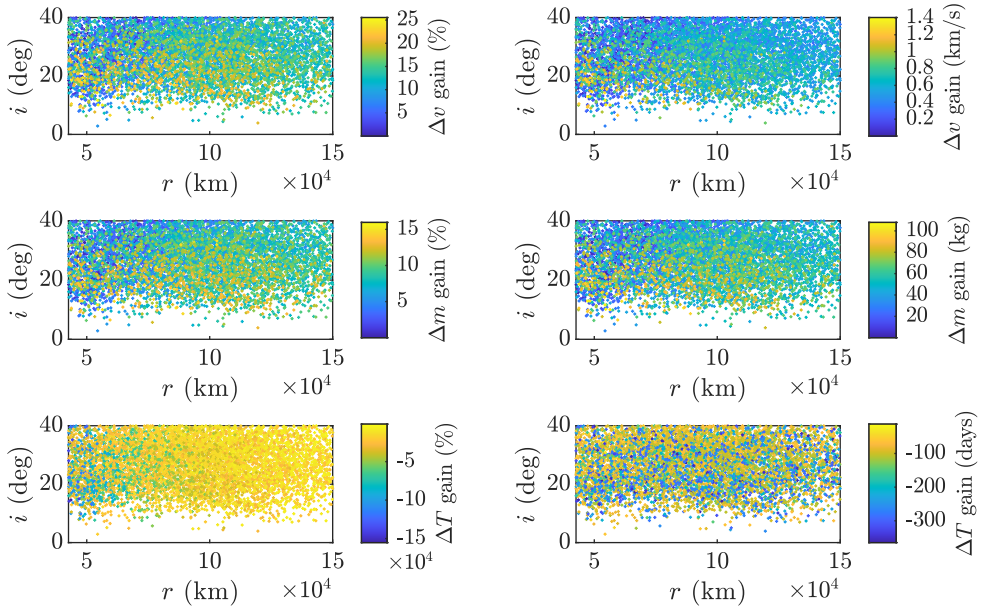

Figure 14: Osculating orbits ϕ_{L} below 150 000 km, with gains in term of manoeuvre costs (Δv), propellant mass consumed (Δm) and time-of-flight (ΔT).

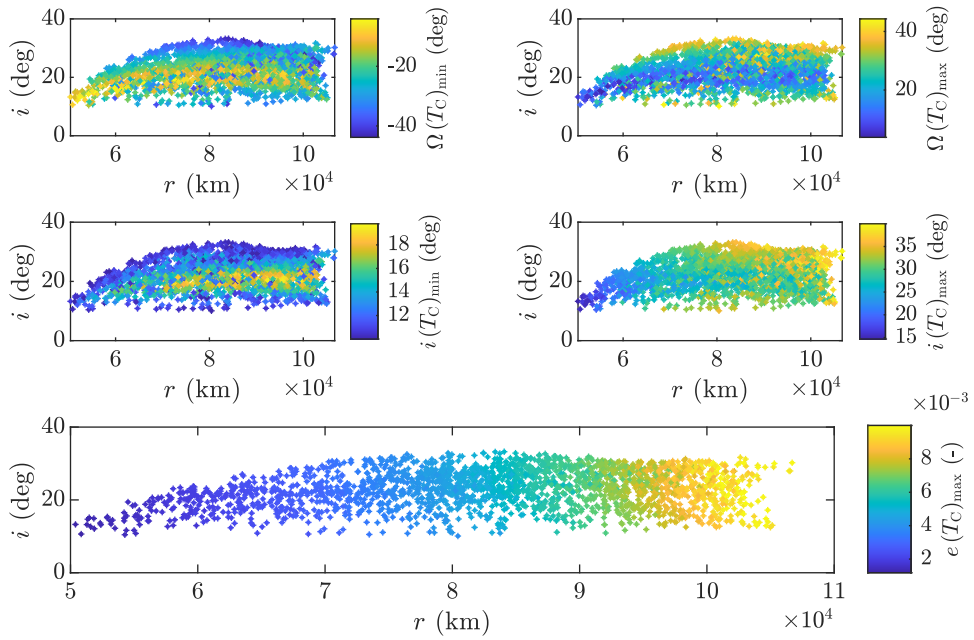

Figure 15: Osculating orbits ϕ_{L} and ϕ_{M} below 150 000 km, with minimum and maximum RAAN and inclination and maximum eccentricity in the time horizon T_{C}.

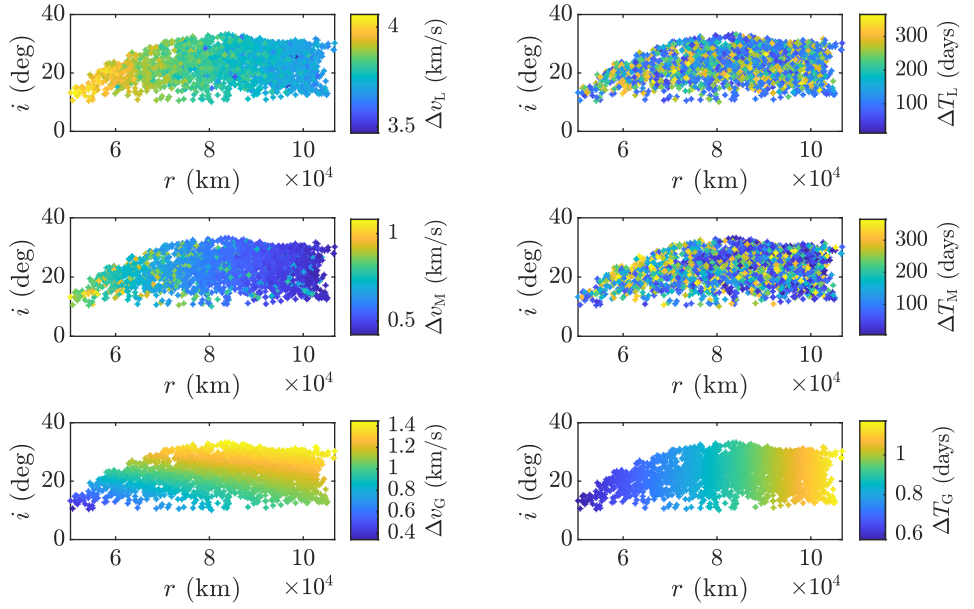

Figure 16: Osculating orbits from LEO, Moon Halo orbits and GSO falling inside the set Ψ_{C} with the associated total manoeuvre cost and time-of-flight.

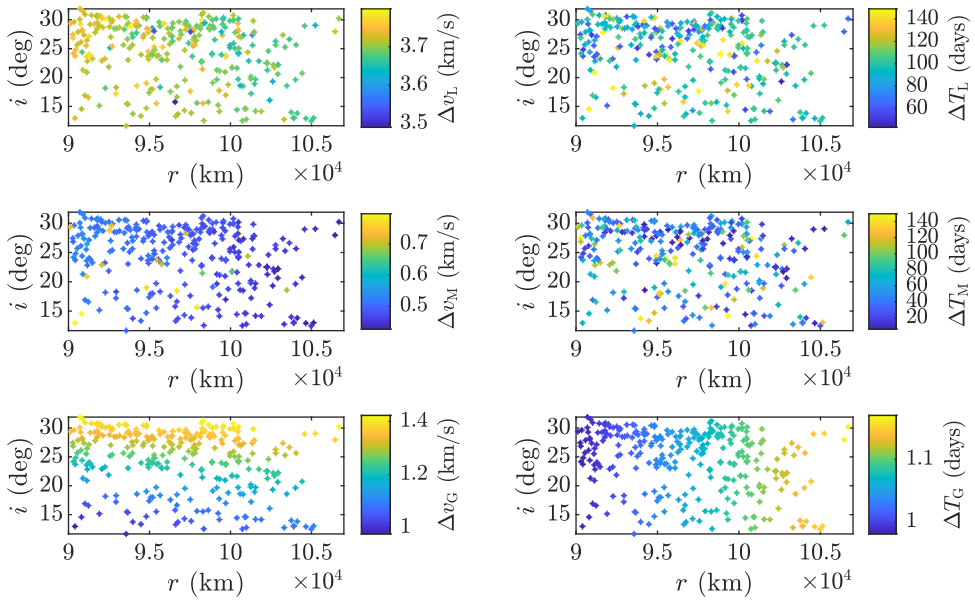

Figure 17: Osculating orbits from LEO, Moon Halo orbits and GSO falling inside the set Ψ_{C} with the associated total manoeuvre cost and time-of-flight below 150 days.

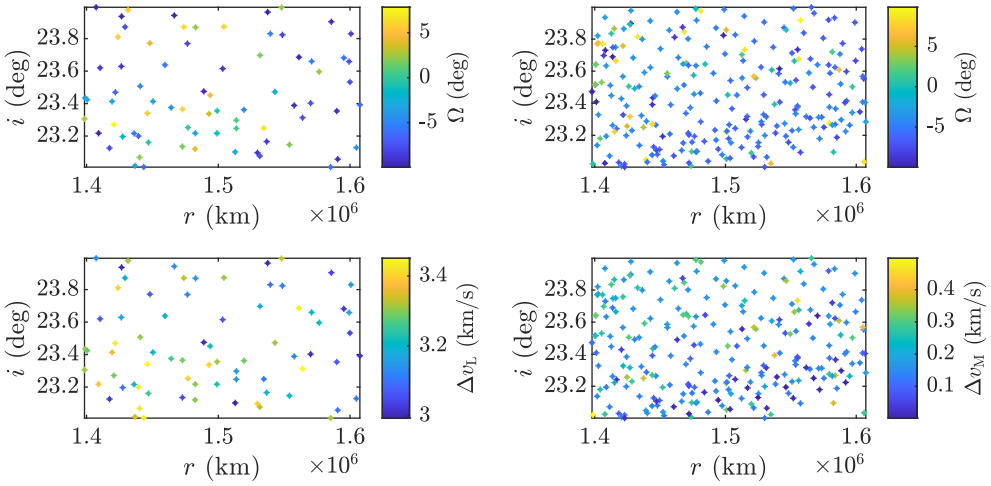

Figure 18: Osculating orbits ϕ_{L} (left) and ϕ_{M} (right) falling inside the reachable set for the Sun–Earth L_1 and L_2 and associated total manoeuvre cost.

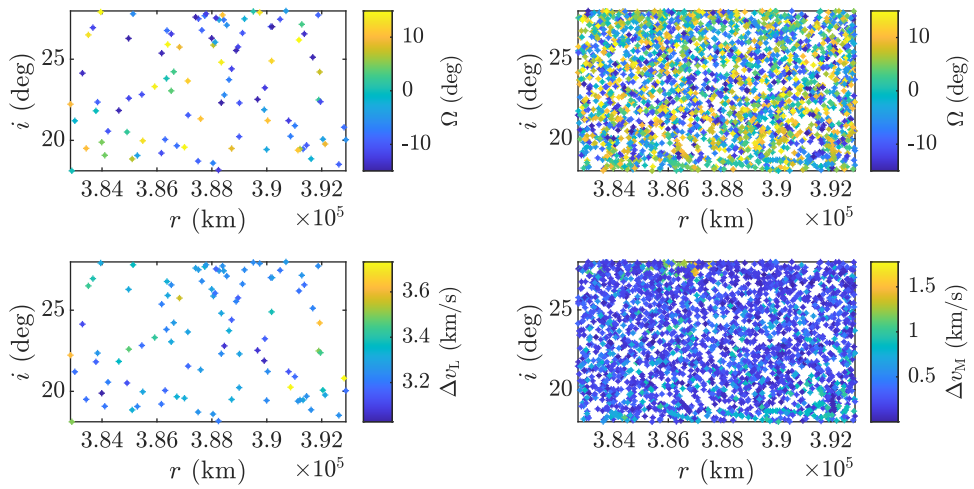

Figure 19: Osculating orbits ϕ_{L} (left) and ϕ_{M} (right) falling inside the reachable set for the Earth–Moon L_4 and L_5 and associated total manoeuvre cost.